Far- and Mid-Infrared of Crystalline 2,2′-Bithiophene: Ab Initio Analysis and Comparison with Infrared Response

P. Hermet,* J.-L. Bantignies, A. Rahmani,[†] and J.-L. Sauvajol

Groupe de Dynamique des Phases Condensées (UMR CNRS 5581), Université Montpellier II, 34095 Montpellier Cédex 5, France

M. R. Johnson

Institut Laue-Langevin, B.P. 156, 38042 Grenoble Cédex 9, France

F. Serein

Hétérochimie Moléculaire et Macromoléculaire, Ecole Nationale Supérieure de Chimie de Montpellier, 34095 Montpellier Cédex 5, France

Received: October 1, 2004; In Final Form: November 23, 2004

Infrared intramolecular vibrations and lattice modes in the crystalline phase of 2,2′-bithiophene (2T) are investigated using the *direct method* combined with density functional theory (DFT)-based total energy calculations. For the first time, the far- and mid-infrared responses have been calculated from the Γ-point modes and the Born effective charge tensors of the 2T crystalline phase. The relative good agreement between the calculated and experimental infrared spectra allows us to assign the origin of the main features of the experimental spectra, which is of particular interest in the far-infrared domain. These assignments are useful for understanding all the properties of the 2T crystalline phase in which phonon−phonon and electron−phonon interactions play an important role.

I. Introduction

Among the conjugated organic polymers, polythiophene has attracted considerable attention for technological applications because of its interesting electronic properties and its excellent chemical stability.[1,2] However, polythiophene presents a number of characteristics, such as low crystallinity and chemical defects, that make it difficult to establish a precise relationship between structure and vibrational dynamics. In this context, oligothiophenes and particularly 2,2′-bithiophene (2T), with a perfectly controlled structure and a short chain length, have become important both as model compounds for polythiophene and as a novel class of molecular materials.[3,4]

Experimental infrared spectra of oligothiophenes constitute a rich source of information about their molecular structure, charge distribution, and conjugational properties. However, even the mid-infrared spectrum of the simplest oligomer, 2T, in the crystalline phase is relatively complex,[5−7] and an unequivocal assignment of modes, in particular at a low frequency, requires theoretical calculations. Ab initio simulations of the infrared spectrum of an isolated 2T molecule were performed by Degli Esposti et al.[5] and compared with the mid-infrared data obtained on a 2T crystalline phase sample. Good agreement was found between the experimental and calculated frequencies for the intramolecular modes in the 300−1600 cm^{-1} frequency range. Nevertheless, because intermolecular interactions were not taken into account in the calculations, the measured intensities were not accurately reproduced. Clearly, from this work, there is no theoretical assignment or experimental data of the far-infrared domain of the 2T crystalline phase.

In this work, a complete experimental infrared investigation (far- and mid-infrared regions) of the 2T crystalline phase, performed over a large temperature range (9−300 K), is reported. To understand these data, infrared spectral simulations of the 2T crystalline phase were performed from first-principles calculations using density functional theory[8,9] (DFT) coupled to the *direct method*.[10] An accurate calculation of the infrared spectrum requires both a good structural and dynamical model as well as knowledge of the Born effective charge tensors (BECTs). The structural and dynamical model of the 2T crystalline phase has already been shown to be in excellent agreement with inelastic neutron scattering (INS) measurements.[11] However, in the literature and to the best of our knowledge, there is no calculation of the BECTs of the 2T crystalline phase or more generally for thiophene oligomers. Accurate calculation of BECTs in organic solids is challenging, since the effective charges are small and high numerical precision is required.

The principal aim of this study is therefore to investigate the infrared active vibrational dynamics of the 2T crystalline phase. Results obtained previously for the normal modes, and calculations of the BECTs, allow us to assign the low-frequency vibrational modes. In addition, since our simulations include intermolecular interactions, this study can confirm the assignments of the high-frequency vibrational modes obtained from the literature using an isolated 2T molecule model.

This paper is organized as follows. In section 2, the temperature dependence of the experimental mid- and far-infrared spectra are presented and analyzed. In section 3, we describe the computational details of our first-principles calculations and we give the fundamental equations for calculating the

† Permanent address: Département de Physique, Université MY Ismail, Faculté des Sciences, B.P. 4010, 50000 Meknés, Morocco.
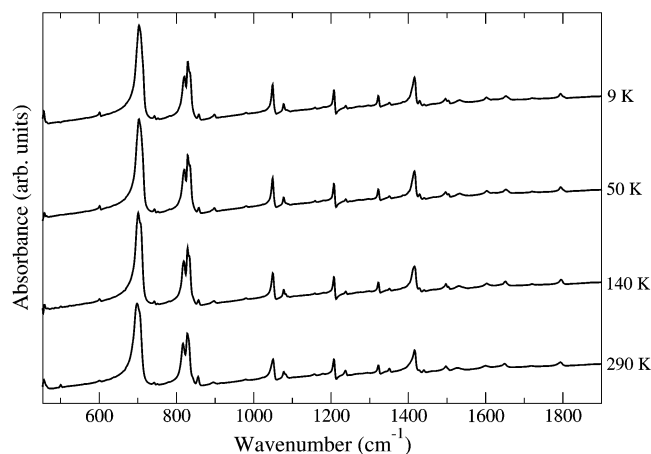
Far- and Mid-Infrared of Crystalline 2,2′-Bithiophene

J. Phys. Chem. A, Vol. 109, No. 8, 2005 **1685**

Figure 1. Experimental mid-infrared spectra of 2T in the 9−290 K temperature range.

infrared spectra. Section 4 presents our computational results. We compare our calculated structural parameters with the experimental ones and those from our previous theoretical calculations. Using the modern theory of polarization based on geometric quantum phase concepts, the BECTs of the 2T crystalline phase are given. In the discussion, the calculated and experimental spectra are compared and a vibrational assignment at the Γ-point ($q = 0$) of the Brillouin zone is proposed for the main infrared bands over the whole spectral range. Finally, our results are summarized in section 5.

II. Experimental Section

A. Experimental Setup. 2T was synthesized by a Ni^0 catalyzed Kumada−Corriu cross-coupling of 2-thienylmagnesium bromide and of 2-bromothiophene. In a nitrogen atmosphere, a solution of 2-bromothiophene (3.5 M, 1 equiv) and of $Ni(PPh_3)_2Cl_2$ (2 mol %) was prepared in dry diethyl ether. The 2-thienylmagnesium bromide, freshly prepared in ether, was added dropwise to this solution over 40 min. After the addition, the reaction was refluxed for 4 h and then stirred at room temperature overnight. After classical workup, the crude product was purified by distillation under vacuum ($Eb_{10} = 403$ K) and 2T was obtained in 72% yield as a yellow-green liquid that immediately crystallizes at room temperature as yellow needles.

Mid- and far-infrared measurements in the 450−4000 and 40−350 cm^{-1} frequency ranges, respectively, were carried out on a Bruker IFS 113V Fourier transform spectrometer. A series of two different beam splitters covered the whole spectral region. A Si bolometer detector cooled at 4 K and a N_2-cooled mercury cadmium telluride (MCT) detector were respectively used to probe the far- and mid-infrared domains with extra sensitivity. The spectral resolution was 4 cm^{-1}, and 64 scans were accumulated for each spectrum. The measurements were performed in the 9−290 K temperature range with a temperature precision of 1 K using a liquid helium cryostat. The 2T material was gently ground with polyethylene powder (10% in concentration) in the far-infrared and with bromide potassium powder (0.5% in concentration) in the mid-infrared. The materials were then pressed into pellets at 8 t to form isotropic pellets with a diameter of 13 mm.

B. Infrared Results. *1. Mid-Infrared Results.* Experimental infrared spectra of the 2T crystalline phase in the mid-infrared domain (450−1900 cm^{-1}) are reported in Figure 1. In this range, the infrared spectrum of 2T at ambient temperature is dominated by relatively sharp intramolecular contributions with an intense band at 698 cm^{-1} and a doublet at 817 and 828 cm^{-1} which

present a shoulder at 833 cm^{-1}. The observed features are in agreement with the published experimental mid-infrared spectra[5−7] at ambient temperature, and the assignment of these bands from the literature is given in Table 1. The spurious bands observed on the high-frequency side of the true absorption at 1049 and 1207 cm^{-1} are due to the Christiansen effect.[12]

Infrared spectra have been collected as a function of temperature in the 9−290 K temperature range. For the intramolecular bands located at 698, 750, 817, 856, 896, and 1159 cm^{-1} and for the frequencies above 1520 cm^{-1} in the experimental spectrum at 290 K, a classical pseudoharmonic behavior is shown with a frequency upshift under cooling of more than 2 cm^{-1}. This classical behavior is related to the strengthening of the effective force constants when the temperature decreases. For the other contributions, the position and width of the bands are insensitive to the temperature, indicating a harmonic behavior.

2. Far-Infrared Results. The temperature dependence of the 2T far-infrared spectra in the crystalline phase is displayed in Figure 2 in the 40−180 cm^{-1} frequency range. The temperature dependence of the mode frequencies is reported in Figure 3 for the most clearly resolved contributions. By contrast with the modes in the mid-infrared range, a strong anharmonic behavior of the vibrational modes is clearly shown. The intensity of each band increases as the temperature decreases, and the position of all vibrational modes presents a frequency upshift under cooling. The broad band observed around 135 cm^{-1} at ambient temperature is much better resolved at 9 K with three contributions which appear at 133, 143, and 149 cm^{-1}. The bands at 119 and 161 cm^{-1} are not visible at 290 K and become evident at 9 K.

The low-frequency modes are well-known to be very sensitive to the structural order. The modes in the far-infrared range in the oligomer thiophene type compounds correspond in general to intercycle librations and/or external lattice modes. However, no accurate experimental or theoretical assignment of the far-infrared modes of the 2T crystalline phase exist to our knowledge in the literature. In consequence, a detailed study of the far-infrared dynamics is performed in section 4 by using first-principles calculations.

III. Computational Details

A. First-Principles Calculations. In the crystalline phase of 2T, calculations of the optimized structure, Hellmann−Feynman forces, and BECTs were performed by using the Vienna ab initio simulation package[13−15] (VASP) and the generalized gradient approximation (GGA) to the exchange-correlation functional as proposed by Perdew, Burke, and Ernzerhof[16] (PBE). The interactions between ions and electrons were described by the projector augmented wave (PAW) method[17] in the real space representation. A $6 \times 6 \times 6$ Monkhorst−Pack[18] k-points mesh over the Brillouin zone was found to provide sufficient precision in the calculation of the geometry optimization and Hellmann−Feynman forces.

Calculation of the dynamical matrix and normal modes of vibrations at the Γ-point were calculated, via the Hellmann−Feynman forces, in the harmonic approximation using the *direct method*[10] implemented in the PHONON software.[19] A detailed discussion on the computational parameters for the construction of the dynamical matrix of the 2T crystalline phase can be found in our previous work.[11]

BECTs are obtained from finite differences of polarizations as various sublattice displacements are imposed with the electronic part of the polarization computed using Berry's phase

1686 *J. Phys. Chem. A, Vol. 109, No. 8, 2005*

Hermet et al.

TABLE 1: Experimental and Calculated Mid-Infrared Frequencies of 2T with Their Assignments[a]

frequency (cm^{-1})			approximate assignment			
			literature		this work	
experimental	calculated	error (%)	assignment[a]	reference	assignment[a]	symmetry
456	452	0.9			$\gamma(C_\alpha\!-\!S\!-\!C_\alpha)$	B_u
	562				$\gamma(C_\alpha\!=\!C_\beta\!-\!C_\beta)$	B_u
601	595	1.0	$\delta(C_\alpha\!-\!S\!-\!C_\alpha)$	25	$\delta(C_\alpha\!-\!S\!-\!C_\alpha)$	B_u
703	674	4.1	$\gamma(C\!-\!H)$	26	$\gamma(C\!-\!H)$	A_u
743	738	0.7	$\nu(C_\alpha\!-\!S)$	25	$\delta(ring)$	B_u
821	797	2.9			$\omega(C\!-\!H)$	B_u
829	831	0.2			$\delta(C_\alpha\!-\!S\!-\!C_\alpha)$	A_u
835	834	0.1			$\delta(S\!-\!C_\alpha\!=\!C_\beta)$	B_u
858			$\delta(ring) + \nu(C\!-\!S)$	25		
898	883	1.7			$\gamma(C_\beta\!-\!H)$	B_u
980			$\delta(ring)$	25		
1049	1055	0.6	$\delta(C_\beta\!-\!H)$	25	$\delta(C_\alpha\!-\!H)$	A_u
1077	1070	0.6	$\delta(C_\alpha\!-\!H)$	25	$\delta(C_\beta\!-\!H)$	B_u
1159						
1207	1188	1.6			$\delta(C_\alpha\!=\!C_\beta\!-\!H)$	A_u
1238	1191	3.8	$\delta(C_\beta\!-\!H)$	25	$\delta(C_\alpha\!=\!C_\beta\!-\!H)$	B_u
1322	1314	0.6			$\delta(ring)$	B_u
1351			$\nu(C_\beta\!-\!C_\beta)$	25		
1416	1443	1.9	$\nu_s(C_\alpha\!=\!C_\beta)$	6,25	$\nu_s(C_\alpha\!=\!C_\beta)$	B_u
1429						
1441						
1496	1492	0.3	$\nu_{as}(C_\alpha\!=\!C_\beta)$	6,25	$\nu_{as}(C_\alpha\!=\!C_\beta)$	B_u
1504	1500	0.3			$\nu_{as}(C_\alpha\!=\!C_\beta)$	A_u
1533					overtones or combination bands	
1602					overtones or combination bands	
1653					overtones or combination bands	
1720					overtones or combination bands	
1794					overtones or combination bands	

[a] Only the fundamental vibrational modes at frequencies smaller than 1800 cm^{-1} are reported. [b] ν = stretching, δ = in-plane bending, ω = wagging, γ = out-of-plane bending, s = symmetric, as = antisymmetric.
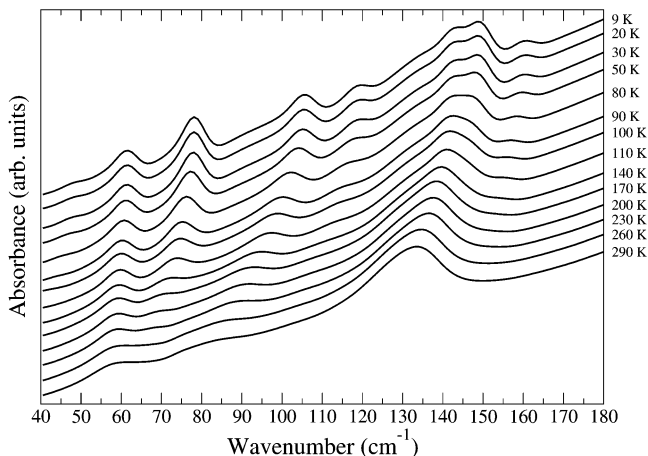
Figure 2. Experimental far-infrared spectra of 2T in the 9−290 K temperature range.
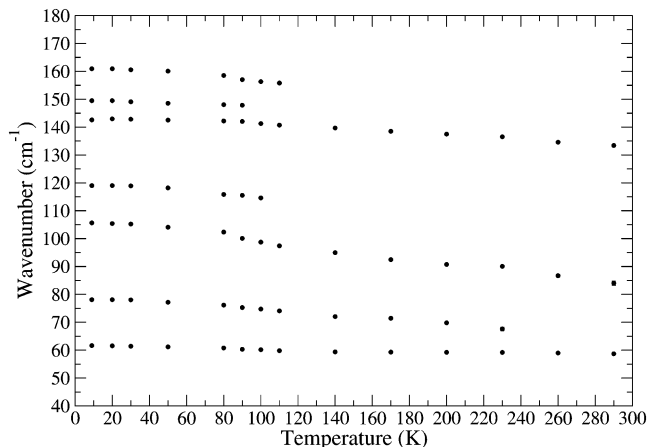

Figure 3. Temperature dependencies of the far-infrared modes. Only the most resolved bands are reported. The error bars are symbolized by the size of the circles.

method as formulated by King-Smith and Vanderbilt.[20] In particular, we have calculated the electronic contribution to the polarization change using a two-dimensional 6 × 6 Monkhorst−Pack perpendicular $k_\perp$-points mesh and a chain of 12 k-points in the parallel direction. Each atom of the asymmetric unit of 2T is displaced by 0.05 Å in each Cartesian direction to compute BECTs (and Hellmann−Feynman forces) by finite difference.

All our calculations were performed with the VASP high-precision option, and a plane-wave energy cutoff of 350 eV was used. With respect to our previous work,[11] it was necessary to use a denser k-point grid and to increase the plane-wave energy cutoff by 25% to ensure the convergence of the BECTs.

DFT calculations were also performed on an isolated 2T molecule by using the GAUSSIAN package[21] with the PBE exchange-correlation functional and the 6-31G(d) basis set. This

package calculates directly the infrared spectrum. Geometry optimization of the 2T molecule was performed until the maximum of residual force on each atom was <3 × 10^{-4} eV/Å.

B. Infrared Spectrum Modeling. The infrared absorption coefficient (α) of an isotropic material is directly related to the imaginary part of the dielectric susceptibility tensor ($\chi''(\mathbf{q}, \omega)$), with $\mathbf{q} = 0$, and can be described by the following expression:

$$\alpha(\omega) = \frac{\omega}{3nc}\sum_\gamma \chi''_{\gamma\gamma} \tag{1}$$

where n and c are respectively the index of refraction of the material and the speed of light and the Greek characters denote

Far- and Mid-Infrared of Crystalline 2,2′-Bithiophene

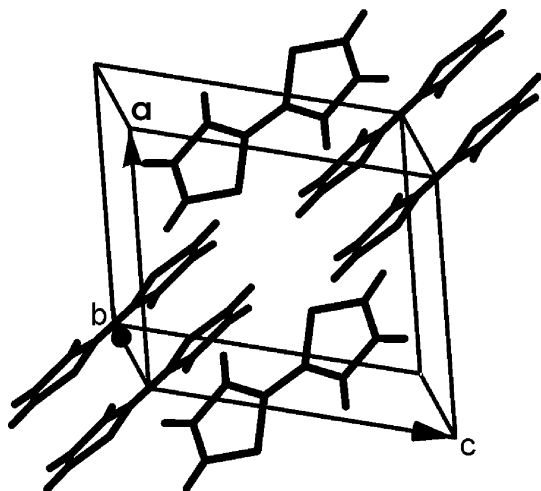*J. Phys. Chem. A, Vol. 109, No. 8, 2005* **1687**

Figure 4. Single crystal of 2T and crystal axis reference system.

the Cartesian components. For harmonic systems, it is possible to show that the imaginary part of the dielectric susceptibility is correlated to the displacement−displacement correlation function and can be defined as a function of the eigenvalues and eigenvectors of the dynamical matrix according to[22]

$$\chi''_{\gamma\gamma}(\omega) = \frac{1}{\epsilon_0 V} \sum_j \frac{S_{\gamma\gamma}(j)}{2\omega_j}[\delta(\omega - \omega_j) - \delta(\omega + \omega_j)] \quad (2)$$

where ω_j, V, and ϵ_0 are respectively the frequency of mode j, the volume of the primitive unit cell, and the vacuum permittivity. In our calculations, the Dirac distribution ($\delta(x)$) is defined as

$$\delta(x) = \lim_{\epsilon \to 0^+} \frac{1}{\pi} \frac{\epsilon}{x^2 + \epsilon^2}, \forall x \quad (3)$$

The mode-oscillator strength tensor ($S_{\gamma\gamma}(j)$) is given by the equation

$$S_{\gamma\gamma}(j) = \left| \sum_{\alpha,n} \frac{Z^*_{\gamma\alpha}(n)}{\sqrt{m_n}} e_\alpha(n, j) \right|^2 \quad (4)$$

where Z^* and m_n are respectively the Born effective charge tensor[23] and the mass of atom n, whereas $e_\alpha(n, j)$ is the αn component of the eigenvector of mode j.

The eigenvectors are normalized by the condition

$$\sum_{\alpha,n} e_\alpha(n, j) e_\alpha(n, j') = \delta_{jj'} \quad (5)$$

where $\delta_{jj'}$ is the Kronecker delta symbol.

IV. Computational Results and Discussion

A. Structure Relaxation. 2T ($C_8H_6S_2$) crystallizes in the monoclinic space group $P2_1/c$ (C_{2h}^5) with two molecules per unit cell.[24] The experimental values of the lattice constants are $a = 7.734$ Å, $b = 5.729$ Å, and $c = 8.933$ Å, and the monoclinic angle (β) is equal to 106.72°. The asymmetric unit of 2T is constituted of eight atoms. Experimentally, the centrosymmetric molecule of 2T is planar and the sulfur atoms adopt a trans configuration (Figure 4).

Since infrared absorption uses long wavelength light, only some modes at the center of the Brillouin zone (Γ-point) are infrared active in the crystalline phase, and these modes are

TABLE 2: Optimized Structural Parameters of the 2T Crystalline Phase

	experimental[a]	simulation[b]
Bond Lengths (Å)		
S_1-C_2	1.713	1.734 (1.735)
$C_2=C_3$	1.432	1.390 (1.392)
C_3-C_4	1.444	1.420 (1.422)
$C_4=C_5$	1.357	1.380 (1.382)
C_5-S_1	1.698	1.715 (1.715)
$C_2-C_{2'}$	1.448	1.444 (1.445)
Angles (deg)		
$S_1-C_2=C_3$	112.5	110.3 (110.3)
$C_2=C_3-C_4$	108.0	113.0 (113.0)
$C_3-C_4=C_5$	114.9	112.5 (112.5)
$C_4=C_5-S_1$	112.1	111.6 (111.6)
$C_5-S_1-C_2$	92.5	92.6 (92.6)
$S_1-C_2-C_{2'}$	121.2	120.8 (120.8)
$C_3=C_2-C_{2'}$	126.4	128.9 (128.9)
Dihedral Angles (deg)		
$S_1-C_2-C_{2'}-S_{1'}$	180.0	180.0 (180.0)
$C_3=C_2-C_{2'}=C_{3'}$	180.0	180.0 (180.0)

[a] Reference 24. [b] The values in parentheses are taken from our previous ab initio optimization.[11]
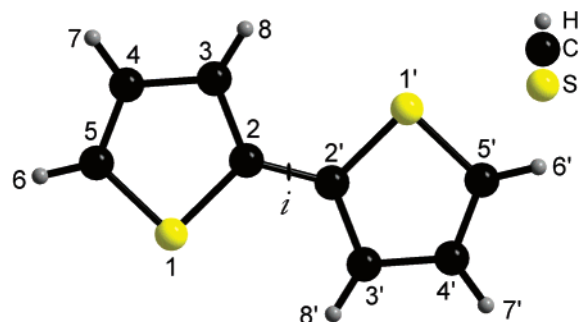

Figure 5. 2T molecule with atom numbering scheme. Primed atoms are related to unprimed ones by an inversion center (i) at the midpoint of the $C_2-C_{2'}$ bond. For the carbon atoms, positions 5 and 2 are also called α-positions or C_α, whereas positions 4 and 3 are called β-positions or C_β.

calculated exactly from a single unit cell. Thus, the experimental unit cell of 2T[24] was optimized by using a fine integration grid on the atomic coordinates until the maximum residual force on each atom was $<3 \times 10^{-4}$ eV/Å. However, since DFT-based methods underestimate dispersive interactions that determine the unit cell shape and size, the experimental unit cell was imposed in the calculations and only the atomic coordinates were optimized. Since the eigenvalues of the dynamical matrix (ω_j^2) obtained for all the vibrational modes are positive both for the isolated molecule and for the crystalline phase, our optimized structures are thermodynamically stable. Table 2 summarizes the geometric parameters obtained after the atomic relaxation of the 2T crystalline phase, which are compared to experimental X-ray diffraction data and to our previous ab initio results. The atom labels and numbering of 2T crystal related to Table 2 are given in Figure 5. Although we have used in this work a denser k-point grid and increased by 25% the cutoff energy for plane waves, the optimization of the atomic coordinates gives bond lengths and angles in perfect agreement with our previous calculations, which were within 1−3% of the measured values except for the $C_2=C_3-C_4$ angle.

B. Born Effective Charges. For insulators, the Born effective charge tensor ($Z^*_{\alpha\beta}(n)$) (also called the transverse charge or dynamical charge) is defined as the proportionality coefficient relating, at the linear order, the macroscopic polarization (P_α) per unit cell, created along the direction α, and the displacement

1688 *J. Phys. Chem. A, Vol. 109, No. 8, 2005*

Hermet et al.

along the direction β of the atoms belonging to the sublattice n under the condition of zero electric field

$$Z^*_{\alpha\beta}(n) = \frac{V}{|e|} \frac{\partial P_\alpha}{\partial u_\beta(n)}\bigg|_{E=0} \qquad (6)$$

where V and e are respectively the volume of the unit cell and the electronic charge. For practical purposes, the Born effective charge is generally decomposed into two contributions: the contribution of nuclei ($Z(n)$) and the contribution due to the electrons ($Z^{el}_{\alpha\beta}(n)$), so that

$$Z^*_{\alpha\beta}(n) = Z(n)\delta_{\alpha\beta} + Z^{el}_{\alpha\beta}(n) \qquad (7)$$

A straightforward approach for the determination of the BECTs consists of computing the difference in macroscopic polarization between a reference state and a state where the atoms belonging to the sublattice n have been displaced by a small but finite distance ($\Delta u_\beta(n)$) (equal to 0.05 Å in this work). Under these conditions, the electronic contribution to Z^* is obtained by the following equation

$$Z^{el}_{\alpha\beta}(n) = \frac{V}{|e|} \frac{\Delta P^{el}_\alpha}{\Delta u_\beta(n)} \qquad (8)$$

where the change in electronic polarization (ΔP^{el}_α) has been identified by King-Smith and Vanderbilt as a geometric quantum phase (or Berry's phase) of the valence wave functions.[20]

The form of the BECTs results directly from the site symmetry of the ions. The unit cell of the 2T crystalline phase is composed of an asymmetric unit of eight atoms which belongs to the C_{2h} point group in the monoclinic $P2_1/c$ space group. When the symmetry operations of the monoclinic space group are applied, each atom of the 2T asymmetric unit appears four times in the unit cell: first at a representative Wyckoff position (x, y, z) and the three others at partner positions $(-x, -y, -z)$, $(-x, 1/2 + y, 1/2 - z)$, and $(x, 1/2 - y, 1/2 + z)$, given by the action of the space group operations: I, $\{C_2^y|0, 1/2, 1/2\}$, and $\{M_y| 0, 1/2, 1/2\}$. Thus, the resulting BECTs are neither diagonal nor symmetric. Our results for the BECTs related to the asymmetric unit of the 2T crystalline phase are presented in Table 3. The Born effective charges for the other atoms can be obtained from those shown in Table 3 by applying the symmetry operations expected by the monoclinic space group. Namely, the BECTs should be identical for partners at $(-x, -y, -z)$, and the off-diagonal xy, yx, yz, and zy matrix elements should change sign for the partners at $(-x, 1/2 + y, 1/2 - z)$ and $(x, 1/2 - y, 1/2 + z)$.

It is obvious from Table 3 that the matrix elements of the BECTs are small. Consequently, the main difficulty in calculating the BECTs of the 2T crystalline phase arises from the numerical precision and thus the high computational cost required to obtain the convergence of these tensors. Because of the finite number of plane waves and the k-point sampling, the acoustic sum rule, $\sum_n Z^*_{\alpha\beta}(n) = 0$, was verified in our calculations within a slight deviation from charge neutrality which is <0.03 electronic charge units.

Although it is not possible to compare directly our effective charge tensors obtained on the 2T crystalline phase with the scalar values obtained by the Mulliken population analysis on the isolated 2T molecule, it is instructive to compare the trace of the computed effective charge tensors with the Mulliken charges (Table 3). The trace of the Born effective charge on the hydrogen atoms has a slightly positive charge which is very

TABLE 3: Born Effective Charge Tensors (Z^*) and Averages of Eigenvalues (λ) for the 2T Crystalline Phase and Mulliken Charges for an Isolated 2T Molecule (in $|e|$)

atom	Z^*			λ	Mulliken
H_6	0.19	0.03	−0.12	0.17	0.18
	0.05	0.18	0.01		
	−0.02	−0.06	0.12		
H_7	0.22	−0.06	−0.11	0.12	0.15
	0.01	0.07	−0.10		
	−0.07	−0.11	0.07		
H_8	0.12	0.06	−0.08	0.14	0.16
	0.09	0.10	0.01		
	−0.13	0.08	0.19		
C_5	−0.51	−0.21	−0.19	−0.26	−0.37
	−0.06	0.07	0.3		
	−0.17	0.14	−0.36		
C_4	−0.26	0.05	0.04	−0.21	−0.11
	0.05	−0.23	0.06		
	0.02	0.05	−0.14		
C_3	−0.09	−0.04	0.09	−0.21	−0.14
	−0.09	−0.34	−0.07		
	0.10	−0.10	−0.19		
C_2	0.16	−0.19	0.22	0.18	−0.17
	−0.26	0.21	0.02		
	0.21	0.08	0.16		
S_1	0.16	0.07	0.14	0.08	0.29
	−0.01	−0.06	−0.19		
	0.06	−0.04	0.15		

close to the Mulliken charge. The charges on the sulfur atoms are positive for both the 2T crystalline phase and the isolated molecule, indicating that the sulfur atom within a thiophene ring is a π-electron donor. Consequently, to ensure the charge neutrality of the system, the carbon atoms of the π-conjugated backbone are negatively charged except for the carbon atoms placed in the α-position in the intercycle bond which is charged positively in the crystalline phase (see Figure 5 for the atom labels). Both for the 2T crystalline phase and for the isolated molecule, larger negative charges are found for the carbon atoms placed at the end α-positions of the thiophene rings, indicating that the electron delocalization is more effective at the center of the molecule.

In the literature and to the best of our knowledge, there is no calculation of the Born effective charge on the 2T crystalline phase or, more generally, on thiophene oligomers. Consequently, the validity of our BECTs must be established by the direct comparison between the calculated and experimental infrared intensities.

C. Comparison of Calculated Infrared Spectra with Experiments. According to section 3, the infrared spectra calculations are a function of the eigenvalues and eigenvectors of the dynamical matrix and of the BECTs. Consequently, we have divided the calculations of the infrared spectra into two steps. In the first step, we have used the group theory to confirm the validity of the dynamical matrix calculation at the Γ-point. Since the structure of the 2T crystalline phase has the point group symmetry C_{2h}, we can demonstrate, within the group theory framework, that the eigenvectors of the dynamical matrix corresponding to the normal mode j at the Γ-point transform according to the irreducible representation of the point group symmetry C_{2h}. Consequently, the dynamical matrix at the Γ-point allows the frequency position of the infrared active modes to be determined without any knowledge of the effective charges on the atoms. Good agreement between the frequencies of infrared active modes and the experimental ones therefore confirms the validity of the dynamical matrix calculations. In the second step, we have calculated the mode-oscillator strength tensors using the BECTs according to eq 4, and the theoretical
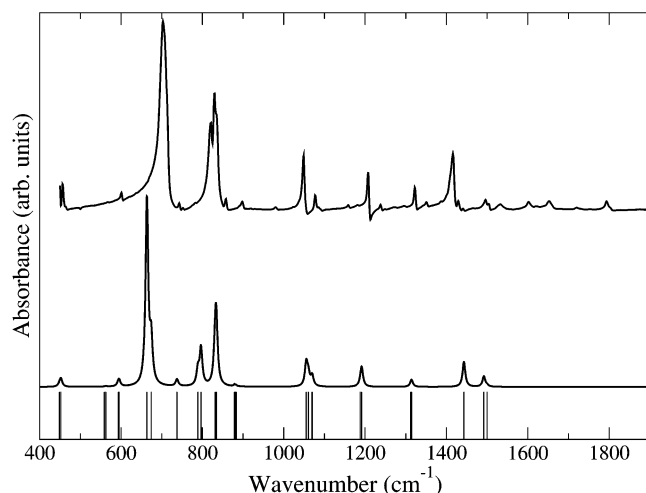
Far- and Mid-Infrared of Crystalline 2,2′-Bithiophene

J. Phys. Chem. A, Vol. 109, No. 8, 2005 **1689**

Figure 6. Experimental (top) and calculated (middle) mid-infrared spectrum of 2T. The vertical bars at the bottom correspond to the theoretical frequencies of the mid-infrared active modes issued from the direct diagonalization of the dynamical matrix. The experimental spectrum displayed in this figure is at 9 K, and a baseline correction has been done for the presentation. The calculated spectrum has been normalized on the experimental band centered at 703 cm^{-1}.

Figure 7. (A) Experimental (top) and calculated (middle) far-infrared spectrum of 2T. The vertical bars at the bottom correspond to the theoretical frequencies of the far-infrared active mode issued from the direct diagonalization of the dynamical matrix. The experimental spectrum displayed in this figure is at 9 K, and a baseline correction has been done for the presentation. The calculated spectrum has been normalized on the experimental band centered at 78 cm^{-1}. (B) Calculated far-infrared spectrum of an isolated 2T molecule.

infrared absorption spectra are calculated from eq 1. The line shape of each vibrational band is assumed to be Lorentzian (eq 3), and the line width (ϵ) is fixed at 3 and 4 cm^{-1}, respectively, for the calculated far- and mid-infrared spectra. To compare the calculated infrared spectra with the experimental ones, the calculated intensities are normalized on the most intense and resolved experimental lines located at 78 cm^{-1} in the far-infrared spectrum and at 703 cm^{-1} in the mid-infrared spectrum.

1. High-Frequency Modes. Figure 6 compares the calculated infrared spectrum of the 2T crystalline phase in the 400–1900 cm^{-1} frequency range with the experimental one measured at 9 K. The positions of the symmetry-allowed infrared active modes are shown, and these are in good agreement with the experimental frequencies, with the largest discrepancies being 4.1% (Table 1). The calculated spectral intensities are also in good agreement with the measured intensities, allowing reliable mode assignments (see also Table 1).

The calculated 400–900 cm^{-1} frequency range is dominated by one strong band at 674 cm^{-1} and one doublet around 830 cm^{-1}. The splitting of this latter contribution and the relative intensity of these two bands are correctly reproduced by the calculation, although the discrepancy of 2.9% in the frequency position of the calculated band at 797 cm^{-1} leads to an overestimate of the doublet splitting. Analyzing the corresponding eigenvectors, we assigned the experimental band at 703 cm^{-1} to an out-of-plane C—H bending and the doublet modes at 821 and 829 cm^{-1} to a C—H wagging and an in-plane C$_\alpha$—S—C$_\alpha$ bending, respectively, whereas we assigned the shoulder at 835 cm^{-1} on the experimental spectrum to an in-plane S—C$_\alpha$=C$_\beta$ bending. It is interesting to note that a mode predicted at 562 cm^{-1} by the group theory analysis has zero intensity in both the experimental and calculated spectra. All the experimental bands between 900 and 1400 cm^{-1} are well reproduced by the calculations. The calculated 1400–1500 cm^{-1} frequency range is particularly important because both the $\nu_s(C_\alpha{=}C_\beta)$ (1443 cm^{-1}) and $\nu_{as}(C_\alpha{=}C_\beta)$ (1492 cm^{-1}) stretching vibrations are active. Furukawa et al.[6] showed that the intensity ratio of these bands serves as an approximate measure of the conjugation length. These calculated bands are in good agreement with the experimental ones both on the frequency position and on the relative intensities. Thus, the agreement between the computed
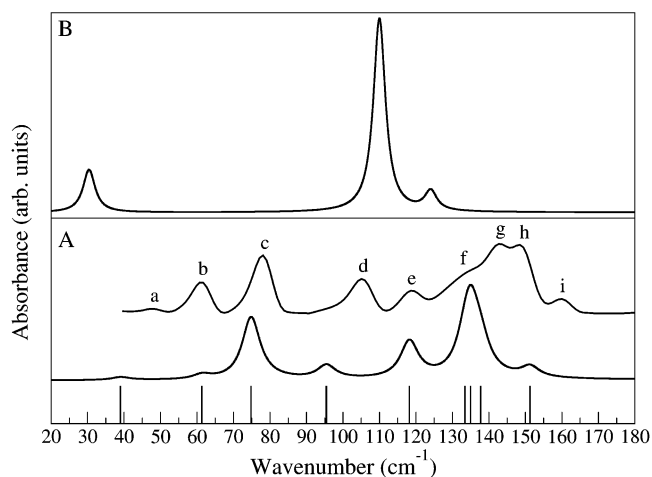
and measured spectra in the mid-infrared range validates the calculation of the BECTs and the intramolecular modes.

Weak features not expected by the group theory are also observed on the experimental spectrum above 1510 cm^{-1} (Table 1). Usually in this frequency range, we can assign these weak bands as overtones or combination bands due to second-order processes. Because experiments have been performed at a low temperature (9 K), only additive combination bands contribute to the infrared spectrum. However, because our calculations are limited to the first-order processes, any comparison with the second-order spectrum is possible. Consequently, this tentative assignment has to be taken with caution.

2. Low-Frequency Modes. The calculated far-infrared spectrum, in the 20–180 cm^{-1} frequency range, of the 2T crystalline phase is compared with the experimental spectrum taken at 9 K (Figure 7). The number of the experimental absorption bands is in agreement with the number of the calculated bands, and generally, the calculated spectral profile bears a good resemblance to the measured profile. Although the level of agreement is not as good as that in the mid-infrared range (Figure 6), we emphasize that, to our knowledge, this is the first calculation of the far-infrared spectrum of the 2T crystalline phase by DFT-based methods.

With the exception of the band centered at 47 cm^{-1}, the positions of the calculated infrared active bands are predicted with a precision better than 10% (Table 4). In terms of intensities, only the modes calculated at 61 and 95 cm^{-1} are significantly underestimated. Despite these shortcomings, the solid state calculation offers a huge improvement over the more commonly performed isolated molecule calculation (Figure 7), which shows only three modes in this frequency range.

Mode assignment (Table 4) of the far-infrared vibrational modes is made on the basis of the calculated spectrum (Figure 8) displaying the atomic vibrations. Since the structure of the 2T crystalline phase has the point group symmetry C_{2h}, the symmetry of the vibrational modes is A$_u$ or B$_u$. For the A$_u$ symmetry, vibrations are parallel to the C_2 symmetry axis which coincides with the b-crystal axis, whereas, for the B$_u$ symmetry, vibrations are on the ac-plane which is a σ-symmetry plane.

The relative good agreement between the calculated and experimental spectra in the mid-infrared range demonstrates the

a **b** **c**

39 cm^{-1} 61 cm^{-1} 75 cm^{-1}

d **e** **f**

95 cm^{-1} 118 cm^{-1} 133 cm^{-1}

g **h** **i**

135 cm^{-1} 138 cm^{-1} 151 cm^{-1}
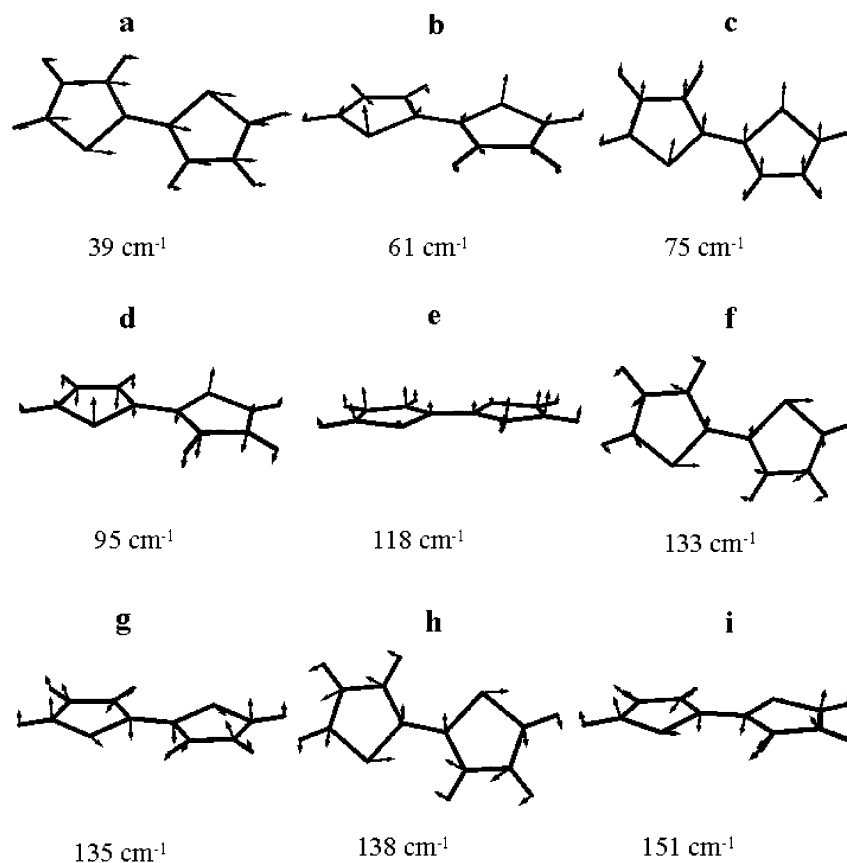
Figure 8. Representation of the far-infrared normal modes of 2T with their calculated frequencies. Band assignments are given in Table 4.

TABLE 4: Experimental and Calculated Far-Infrared Frequencies of 2T with Their Assignments

mode[a]	exptl (cm^{-1})	simulation (cm^{-1})	error (%)	approximate attribution and symmetry[b]
a	47	39	17.0	optical translational mode (A$_u$)
b	62	61	1.6	twist mode (A$_u$)
c	78	75	3.8	optical translational mode (B$_u$)
d	105	95	9.5	twist mode (B$_u$)
e	119	118	0.8	optical translational mode (A$_u$)
f	133	133	0.0	in-plane rotation + out-of-plane bending of thiophene rings (A$_u$)
g	143	135	5.6	butterfly mode (B$_u$)
h	149	138	7.4	in-plane rotation + out-of-plane torsion of thiophene rings (B$_u$)
i	161	151	6.2	butterfly + torsion of thiophene rings (A$_u$)

[a] Band labels are given in Figure 7. [b] Representations of the far-infrared normal modes are given in Figure 8.

accuracy in the calculation of the BECTs and the intramolecular modes. Exactly the same BECTs are used to calculate the low-frequency spectrum. However, the calculated far-infrared spectrum does not agree as well with the measured spectrum. Looking back at the calculated INS phonon spectrum,[11] it shows a good but not perfect agreement between measurement and calculation. In the case of the INS spectrum, a density of states, summed over the whole Brillouin zone, is measured (and calculated), whereas in the case of the infrared spectrum, only the Γ-point modes are relevant. The infrared spectrum is therefore simpler and modes are more clearly resolved, highlighting any shortcomings in the calculation. A first explanation for this disagreement could be related to the lack of dispersive interactions in the DFT method. Indeed, optimization of the cell parameters is unphysical in a van der Waals bonded solid and

applying external pressure by fixing the cell parameters at the measured values is only an approximate solution.

Work currently being undertaken on the bigger molecule α-quaterthiophene (4T),[27] using exactly the same method described in this paper, shows better agreement between the measured and calculated IR spectra than that obtained here for 2T. The disagreement between experiment and simulation may therefore also be experimental in origin. The melting point of 2T (300 K) is close to room temperature, and the yellow powder tended to discolor or darken during preparation of the pellet. Longer oligomers have higher melting points and do not suffer from this effect. Sample preparation of 2T was repeated a number of times, and only pellets showing a minimum of discoloration were retained. Nevertheless, these color changes indicate small changes in the electronic structure due to modification of the solid state structure following melting and recrystallization. Thus, the cooled solid is likely to be a mixture of domains with different degrees of crystallization and some amorphous regions. The calculation has been performed for a perfect powder of 2T. Lattice modes are particularly sensitive to the solid state structure, whereas higher-frequency modes are dominated by intramolecular interactions. One signature of partial crystallization would be inhomogeneous line broadening, as illustrated by the modes around 150 cm^{-1}.

V. Conclusions

We have investigated the structure and the infrared spectra in a wide frequency range (20−1900 cm^{-1}) of the 2T crystalline phase using DFT-based methods. The parameters of the relaxed atomic structure are found to be in very good agreement with the experimental ones. We have calculated the phonon frequencies at the center of the Brillouin zone, the BECTs, and the infrared absorption response of the 2T crystalline phase. We

have found good agreement between the calculated phonon frequencies and their experimental values according to the symmetry properties of the eigenvectors of the dynamical matrix. The Born effective charges are found to be small which is typical of a covalently bonded organic system. The traces of the BECTs indicate that the charges on the hydrogen and sulfur atoms are positive, whereas the charges on the carbon atoms are negative except for the carbon atoms included in the intercycle bond, which are charged positively in the crystalline phase. The good agreement between the calculated and experimental infrared spectra allows us to assign the origin of the main features of the experimental spectra and demonstrates the accuracy of the BECT calculations. In particular, we have proposed for the first time an assignment of the vibrational modes in the far-infrared domain.

In contrast to our previous calculations of the INS spectrum for the 2T crystalline phase, the simpler infrared spectrum at a low frequency reveals problems in the precision of the far-infrared mode calculations, which could be related in part to the lack of dispersive interactions in the DFT methods but also to experimental problems during the preparation of 2T samples.

Recently, this work has been extended to longer oligomers, like α-quaterthiophene and α-sexithiophene, to understand in detail the experimental results (INS and infrared spectra) of these materials.

References and Notes

(1) Roncali, J. *Chem. Rev.* **1992**, *92*, 711.
(2) Hotta, S.; Hosaka T.; Shimotsuma W. *Synth. Met.* **1983**, *6*, 69.
(3) Nalwa, H. S. *Handbook of Organic Conductive Molecules and Polymers*; Wiley: Chichester, U.K., 1997.
(4) Müllen, K.; Wegner, G. *Electronic Materials*: *The Oligomer Approach*; Wiley-VCH: Weinheim, 1998.
(5) Degli Esposti, A.; Zerbetto, F. *J. Phys. Chem. A* **1997**, *101*, 7283.
(6) Furukawa, Y.; Akimoto, M.; Harada, I. *Synth. Met.* **1987**, *18*, 151.
(7) Zerbi, G.; Chierichetti, B.; Ingänas, O. *J. Chem. Phys.* **1991**, *94*, 4637.
(8) Hohenberg, P.; Kohn, W. *Phys. Rev.* **1964**, *136*, B864.
(9) Kohn, W.; Sham, L. J. *Phys. Rev.* **1965**, *140*, A1133.
(10) Parlinski, K. *Am. Inst. Phys. Conf. Proc.* **1999**, *479*, 121.
(11) Hermet, P.; Bantignies, J. L.; Rahmani, A.; Sauvajol, J. L.; Johnson, M. R. *J. Phys.: Condens. Matter* **2004**, *16*, 7385.
(12) Socrates, G. *Infrared and Raman Characteristic Group Frequencies*; Wiley: Chichester, U.K., 2001.
(13) Kresse, G.; Furthmüller, J. *Phys. Rev. B* **1996**, *54*, 11169.
(14) Kresse, G.; Furthmüller, J. *Comput. Math. Sci.* **1996**, *6*, 15.
(15) Kresse, G.; Hafner, J. *Phys. Rev. B* **1993**, *47*, 558.
(16) Perdew, J. P.; Burke, K.; Ernzerhof, M. *Phys. Rev. Lett.* **1996**, *77*, 3865.
(17) Kresse, G.; Joubert, D. *Phys. Rev. B* **1999**, *59*, 1758.
(18) Monkhorst, H. J.; Pack, J. D. *Phys. Rev. B* **1976**, *13*, 5188.
(19) Parlinski, K. *PHONON Software*; Cracow, 2001.
(20) King-Smith, R. D.; Vanderbilt, D. *Phys. Rev. B* **1993**, *47*, 1651.
(21) Frisch M. J.; Trucks, G. W.; Schlegel, H. B.; Scuseria, G. E.; Robb, M. A.; Cheeseman, J. R.; Montgomery, J. A.; Vreven, T.; Kudin, K. N.; Burant, J. C.; Millam, J. M.; Iyengar, S. S.; Tomasi, J.; Barone, V.; Mennucci, B.; Cossi, M.; Scalmani, G.; Rega, N.; Petersson, G. A.; Nakatsuji, H.; Hada, M.; Ehara, M.; Toyota, K.; Fukuda, R.; Hasegawa, J.; Ishida, M.; Nakajima, T.; Honda, Y.; Kitao, O.; Nakai, H.; Klene, M.; Li, X.; Knox, J. E.; Hratchian, H. P.; Cross, J. B.; Adamo, C.; Jaramillo, J.; Gomperts, R.; Stratmann, R. E.; Yazyev, O.; Austin, A. J.; Cammi, R.; Pomelli, C.; Ochterski, J. W.; Ayala, P. Y.; Morokuma, K.; Voth, G. A.; Salvador, P.; Dannenberg, J. J.; Zakrzewski, V. G.; Dapprich, S.; Daniels, A. D.; Strain, M. C.; Farkas, O.; Malick, D. K.; Rabuck, A. D.; Raghavachari, K.; Foresman, J. B.; Ortiz, J. V.; Cui, Q.; Baboul, A. G.; Clifford, S.; Cioslowski, J.; Stefanov, B. B.; Liu, G.; Liashenko, A.; Piskorz, P.; Komaromi, I.; Martin, R. L.; Fox, D. J.; Keith, T.; Al-Laham, M. A.; Peng, C. Y.; Nanayakkara, A.; Challacombe, M.; Gill, P. M. W.; Johnson, B.; Chen, W.; Wong, M. W.; Gonzalez, C.; Pople, J. A. *Gaussian 03*, revision B.03; Gaussian, Inc.: Pittsburgh, PA, 2003.
(22) Maradudin, A. A.; Montroll, E. W.; Weiss, G. H.; Ipatova, I. P. *Theory of lattice dynamics in the harmonic approximation*; Academic Press: New York, 1971.
(23) The asterisk superscript of $Z_{\alpha\beta}^{*}(n)$ is not the symbol for the complex conjugation operation. $Z_{\alpha\beta}^{*}(n)$ is always a real quantity.
(24) Pelletier, M.; Brisse, F. *Acta Crystallogr., Sect. C* **1994**, *50*, 1942.
(25) Louarn, G.; Buisson, J. P.; Lefrant, S.; Fichou, D. *J. Phys. Chem.* **1995**, *99*, 11399.
(26) Akimoto, M.; Furukawa, Y.; Takeuchi, H.; Harada, I. *Synth. Met.* **1986**, *15*, 353.
(27) Hermet, P.; Bantignies, J. L.; Sauvajol, J. L.; Johnson, M. R. Manuscript in preparation.